Microstructure, porosity and roughness of RF sputtered oxide thin films: Characterization and modelization

Fahd Oudrhiri-Hassani, Lionel Presmanes, Antoine Barnabé, Philippe Tailhades *

Institut Carnot CIRIMAT, UPS-INPT-CNRS 5085, Université Paul Sabatier 118, route de Narbonne 31 062 Toulouse Cedex 9, France

A B S T R A C T

Spinel $CoMnFeO_4$ thin films are stable materials useful to study the influence of radio-frequency (RF) sputtering experimental conditions on the microstructure of oxide films. It has been demonstrated by various techniques such as electronic and atomic force microscopy (AFM), gas adsorption techniques and ellipsometry, that films prepared with 0.5 Pa sputtering argon pressure and 5 cm target–substrate distance are very dense. On the other hand, the samples obtained under higher pressure and/or longer distances are microporous with a mean pore size generally lower than 2 nm. The specific surface areas of such films reach about 75 m^2/g.

According to the simple model proposed, the films are made of three layers. From the bottom to the top of the film, the first one at the interface with the substrate is 100% dense. The second layer is made of cylindrical rods set up according to a compact plane. Its porosity is due to the lattice interstices. Hemispheric domes covering each rod make up the third layer, which displays a degree of roughness related to the shape and the hexagonal arrangement of the domes. The surface enhancement factor (SEF), the porosity and roughness, calculated from the model, are in corroboration with the experimental values. The porosity factor is however slightly underestimated by the model for very porous samples.

Keywords:
Spinel oxide
Thin films
Microstructure
Sputtering
Ellipsometry
Surface enhancement factor

1. Introduction

Radio-frequency (RF) sputtered thin films are generally made up of small crystallites which have developed closely in relation to each other, in such a manner that the pores in between can only be very small. It is then very difficult to precisely characterize the microstructure and the porosity of such films. Not only scanning and transmission electron microscopy (SEM, TEM) but also atomic force microscopy (AFM) is generally used to characterize the crystallite and grain size. But these techniques are not well suited to give quantitative information about open and close porosity.

For this reason, physical adsorption isotherms of nitrogen or krypton are sometimes used to determine the surface area of porous thin films, by the Brunauer, Emmet and Teller (BET) method [1]. However, this method is quite difficult to carry out because about 1 m^2 of an effective surface is required for the measurement using volumetric techniques. Only a few studies have been carried out so far for sputtered thin films [2–5]. Effective surfaces of less than 10 cm^2 can be measured using surface acoustic waves (SAWs) detection [6] in place of volumetric systems. Special interdigited electrodes however have to be deposited on the top of the films for these SAW measurements.

Ellipsometry is another interesting technique able to give precise information about the thin film porosity. The volume fraction of adsorbate molecule (nitrogen, ethanol, water, ...) inside the pores can be calculated from the measured change in optical characteristics of the porous film during adsorption/desorption at room temperature or liquid nitrogen temperature [7–9]. In air at room temperature, models for porous materials can also be used to determine the film porosity from the spectral variation of n and k optical indices, in the visible light range [10].

The purpose of this paper is to investigate the fine microstructure of thin films oxide prepared with different RF sputtering conditions and to build a microstructural model which is able to describe the architecture of the films on a nanometric scale. $CoMnFeO_4$ spinel oxide films were chosen for this study because $CoMnFeO_4$ displays a good structural stability and quite a low sensitivity to oxido-reduction phenomena [11]. Any significant change in the phase purity could not then be feared for the sputtering conditions used. Microscopy techniques such as, SEM, TEM and AFM, of course without forgetting conventional surface area measurements and spectral ellipsometry at room tempera-

* Corresponding author. Fax: +33 561556163.
E-mail address: tailhade@chimie.ups-tlse.fr (P. Tailhades).

doi:10.1016/j.apsusc.2008.03.149

Table 1
Experimental conditions carried out for samples preparation

Argon flow rate (cm^3/min)	11	55
Argon pressure (Pa)	0.5	2
Target–substrate distance (cm)	5, 6.5, 8	5, 6.5, 8
Power density (W cm^{-2})	0.9	0.9
Film thickness (nm)	300	300

ture and grazing incidence X-ray diffraction (GIXRD) measurements were carried out to obtain precise microstructural information. From these experimental data a microstructural model could be proposed. The growth process of the film as a function of the elaboration conditions was also discussed in the light of this model.

2. Experimental

2.1. Films preparation

Mixed cobalt manganese ferrite thin films were deposited in an Alcatel A450 RF sputter system from a 10 cm in diameter $CoMnFeO_4$ target. The target was produced starting from commercial oxides with 99.999% purity. A mixture of Co_3O_4, Mn_2O_3 and Fe_3O_4 as required in a 1:3/2:1 proportion was used. The ceramic target, sintered at 1200 °C for 1 h, was made of pure $CoMnFeO_4$ spinel oxide. The Alcatel A450 RF sputter machine was equipped with a radio-frequency-generator (13.56 MHz) device as well as a pumping system (a mechanical pump coupled with a turbo molecular pump) which allows reaching a residual pressure down to 10^{-5} Pa, a gas flow controller, a water cooled target holder, a magnetron placed behind the target and two water cooled sample holders. The films were deposited on glass slides having an average arithmetic roughness lower than 0.5 nm. A residual vacuum of 5×10^{-5} Pa was reached in the sputtering chamber before introducing the deposition gas (argon). In order to obtain various microstructures, different distances and argon pressures were used. For each experimental condition, the target was sputtered for 20 min before starting the film deposition on the glass substrate. The whole experimental conditions used to prepare 300 nm thick films, are summarized in Table 1. In the next part of this publication, the samples will be named "P*x*d*y*", with *x* the value of argon pressure in Pascal, and *y* the sample target distance in centimeter.

3. Characterizations

Film thicknesses were measured using a Dektak 3030ST profilometer. Structural characterizations of films were performed by grazing angle X-ray diffraction (GIRXD) on a Siemens D 5000 diffractometer. The apparent crystallite size determined in θ–2θ mode from the full width at half maximum (FWHM) of (3 1 1) spinel peaks, applying pseudo distribution for the peak broadening, and using the Sherrer formula below, to deduce the apparent crystallite size:

$$\mathrm{FWHM} = \frac{k\lambda}{L\cos\theta}$$

where FWHM is size broadening corrected by the instrumental contribution and k is a constant, in this calculation $k = 0.9$, λ is the radiation wavelength ($\lambda = 1.5406$ Å for Cu Kα_1), L is apparent crystallite size and θ is Bragg angle.

Microscopic studies were carried out with a Veeco Dimension 3000 AFM equipped with a super sharp TESP-SS Nanoworld© tip (nominal resonance frequency 320 kHz, nominal radius curvature 2 nm), a JEOL JSM 6700F field emission gun (SEM) and JEOL USF 2700 transmission electron microscope (TEM).

The surface area measurements were done on freshly prepared samples with a Micromeritics ASAP 2010 operating with Krypton at liquid nitrogen temperature. Several (1.3 cm × 1.3 cm) square samples covered on each side by 300 nm thick oxide films were placed in the Micromeritics ASAP 2010 cell for each experiment. Prior to measurements, the samples were heated under vacuum at 300 °C for 16 h to clean their surfaces [6].

Ellipsometry was also carried out with a spectroscopic ellipsometer Horiba Jobin-Yvon UVISEL™ apparatus in the whole visible spectral range of (350–800 nm), all ellipsometric data were recorded at an incidence angle of 70.4° and were analysed using the Delta-Psi software Version 2.0. The fitting of ellipsometric data, Is($\sin 2\Psi \cdot \sin \Delta$) and Ic($\sin 2\Psi \cdot \cos \Delta$) for the glass substrate and the oxide thin film, was first modelled with the Tauc-Lorentz (TL) dispersion relations [12–14]. A sample stack structure (Fig. 1a), glass/film/surface layer, was employed to extract the optical constants (n and k) of thin films. The glass thickness substrate is fixed at 1 mm and the thickness of film and surface layer are equally fitted.

Most of the films studied are porous and the optical constants measured are related to the properties of both $CoMnFeO_4$ and voids. Some samples however, are almost 100% dense, as demonstrated by surface area measurements and the high values of the refractive and absorptive indices. The real optical constants of dense $CoMnFeO_4$ can then be obtained from these samples. To determine the porosity and to study the evolution of the films, a second model is adopted considering a glass substrate of $L_1 = 1$ mm thickness, covered by the oxide film made itself by two layers L_2 and L_3 (Fig. 1b). The first one called (L_2), in contact with the substrate, is completely dense, its thickness is L_2 nanometers and its optical constants are those previously determined for dense $CoMnFeO_4$. The second layer (L_3) of L_3 nanometers, displays a porosity of p_3 percent. The upper part (L_4) of the film is made of a 50% porous layer having a thickness of L_4 nanometers. Surface roughness and porous layers were modelled with the Bruggeman effective medium approximation (BEMA) [15], where the layers are constituted of a mixture of dense $CoMnFeO_4$ and void.

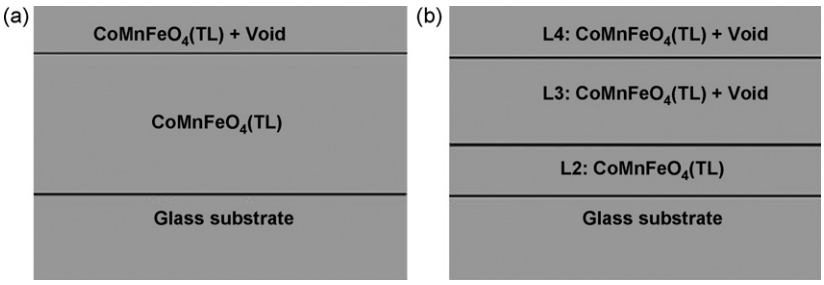

Fig. 1. The layer structure for ellipsometric data analysis (a) EMA model to extract refractive indices (b) EMA model of porous $CoMnFeO_4$ film.

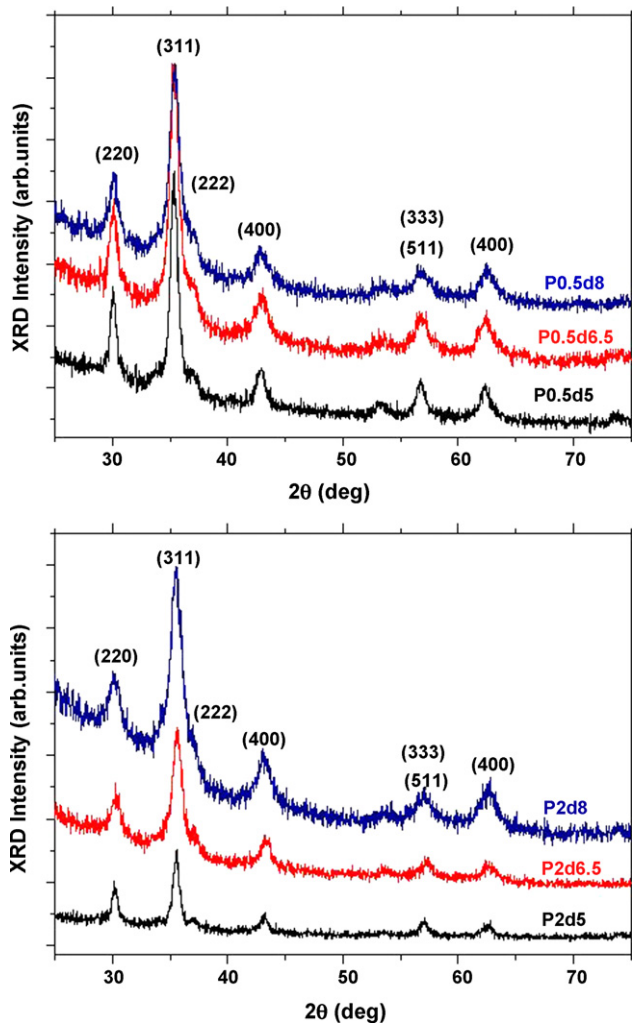

Fig. 2. GIXRD patterns of Pxdy films.

4. Experimental results

The X-ray diffraction patterns (Fig. 2) show the films are all made up of a single cubic spinel phase. For a given argon pressure, the apparent crystallite size seems to be decreased by increasing distance (Table 2). This is mainly due to a lower flux and a lower energy of atoms coming to the film during its growth, for the longest target–substrate distance. The variation of the coherent size of the diffraction domains determined by the X-ray peaks broadening is similar to that obtained by AFM and SEM microscopy techniques (Figs. 3 and 4). Moreover, the mean size of the crystallites is very close to the mean grain size (Table 3). As a result, the grains observed by microscopy techniques are assumed to be single crystals. From AFM or SEM images, it is difficult to clearly reveal pores or interstices between grains or crystallites and to discriminate samples prepared at the same target–substrate 'd*y*' distance but with different argon pressure.

From krypton adsorption isotherms at 77 K (Fig. 5), the surface area can be measured for these samples. It can then be shown that the latter is higher when the sputtering pressure is 2 Pa. If the normalized accessible surface area or surface enhancement factor (SEF) is defined by the surface area measured by krypton adsorption for a 1 m × 1 m square part of a 300 nm thick film, SEF can reach 112 m^2 for P2d8 sample, but it is only 30 m^2 for P0.5d8. In the same manner, the lowering of the target–substrate distance leads to a decrease in SEF making P0.5d5 sample almost free of pore (Table 2). If we assume that the perfectly dense $CoMnFeO_4$ has a density close to 5, the specific surface area of the samples studied is in between 1 and 75 m^2/g approximately. These values are of the same order as those of micronic or submicronic spinel oxides powders.

Ellipsometry allows us to obtain n and k in the visible spectral range (Fig. 6). On several occasions, it has been confirmed that the fitting results were reproducible and physically reasonable. We observed that n and k values changed for materials characterized, this variation is due to the material's porosity. The highest optical constants were then acquired for the samples deposited under the conditions leading to the highest film density, i.e. $P = 0.5$ Pa.

From the first model it has been possible to determine the optical indices of dense $CoMnFeO_4$, which has enabled us to model another stacking layer (Fig. 1b). This allows us to study the microstructure and porosity of thin films deposited under different conditions of deposition. A good fit was always obtained for each sample with minimizing the mean-squares deviation χ^2. Taking into account the three layers model proposed (Fig. 1b), the fit of the curves gives the value of the thickness of each layer and the porosity of the intermediate layer L_3 (Table 2). It is observed that the thickness of the dense layer tends to increase when the target–substrate distance becomes shorter. On the other hand, the porosity of the L_3 part of the film is strongly enhanced for the samples prepared at high pressure. The total thickness of the films remains however approximately the same as the value that was given by the first model (Table 4). Differences of less than 5 nm were only observed.

The R_a arithmetic roughness measured by AFM does not show any significant and meaningful difference for samples prepared at different argon pressures. The roughness is mainly related to crystallite size, which is dependent on target–substrate distance. The rougher samples are then obtained when this distance is close to 5 cm (Table 2).

5. Microstructural model

According to the microscopic observations, ellipsometric analysis and krypton adsorption measurements, a simple model is proposed to describe the microstructural organisation of the

Table 2
Microstructural characteristics of the films: experimental data

Samples	Crystallites diameters determined from X-ray peaks broadening (nm)	Porosity of the L_3 layer from ellipsometry data (%)	L_3 thickness from ellipsometry data (nm)	Average porosity of the film ($L_2 + L_3 + L_4$) (%)	SEF measured from Kr adsorption isotherms (BET method) (m^2)	Arithmetic roughness R_a of the films from AFM measurements (nm)
P0.5d5	17 ± 2	0^{+1}_{0}	0^{+5}_{0}	1.0 ± 0.3	2 ± 0.5	2.1 ± 0.2
P0.5d6.5	15 ± 2	0^{+1}_{0}	0^{+5}_{0}	1.2 ± 0.2	2 ± 0.5	1.8 ± 0.2
P0.5d8	14 ± 2	2 ± 0.5	144 ± 15	2.5 ± 0.5	30 ± 3	1.9 ± 0.2
P2d5	21 ± 3	14 ± 0.6	254 ± 10	12.2 ± 0.3	16 ± 2	2.7 ± 0.2
P2d6.5	16 ± 2	14 ± 2	259 ± 10	12.5 ± 0.3	53 ± 5	1.9 ± 0.2
P2d8	12 ± 2	13 ± 0.6	270 ± 5	12.2 ± 0.2	112 ± 11	1.3 ± 0.2

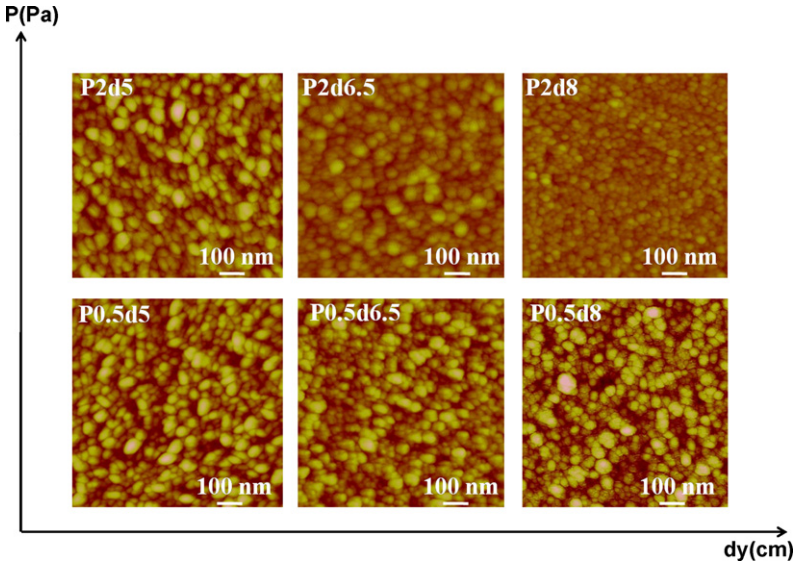

Fig. 3. AFM images of Pxdy films.

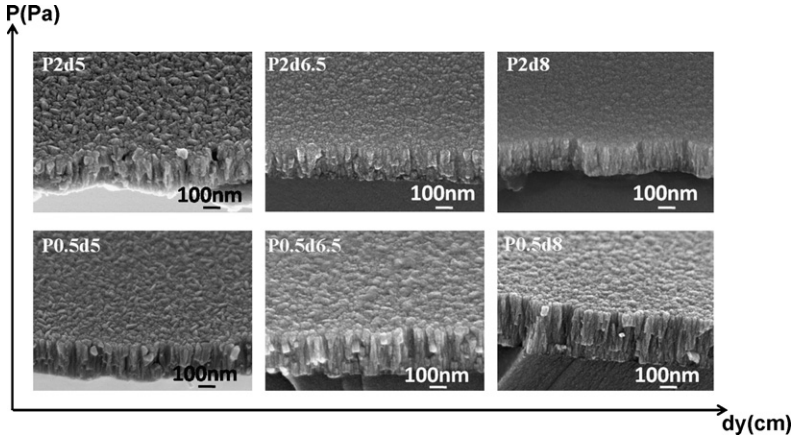

Fig. 4. SEM images of Pxdy films.

films on a nanometric scale. This model assumes that the films are made up of three layers namely L_2, L_3 and L_4 thick, as described previously. The porous L_3 layer is formed by a compact arrangement of cylindrical rods of diameter d. The hemispheric domes, located at the top of the previous cylinders, make up the upper part of the film (L_4 layer) (Fig. 7). The microstructure of the (L_3) and (L_4) layers then looks like the microstructures described by Thornton [16] when the deposition temperature is low.

SEF is the surface on which krypton can be adsorbed for a film of unit area. SEF is the sum of the area of the bottom of the interstices between the rods $(1-\pi/2\sqrt{3})$, the lateral surface area of the rods $(2\pi L_3/d\sqrt{3})$, and the surface area of the domes $(\pi/\sqrt{3})$ (details of calculation are given in Appendix A). It can then be written as:

$$\mathrm{SEF} = \frac{(4L_3 + d)\pi + 2d\sqrt{3}}{2d\sqrt{3}} \tag{1}$$

Table 3
Comparison of grain size measured by SEM, AFM and XRD techniques

Samples	SEM grain size (nm)	AFM grain size (nm)	XRD crystallite size (nm)
P0.5d5	22 ± 5	25 ± 6	17 ± 2
P0.5d6.5	21 ± 5	24 ± 6	15 ± 2
P0.5d8	17 ± 4	22 ± 5	14 ± 2
P2d5	22 ± 5	25 ± 6	21 ± 3
P2d6.5	15 ± 4	21 ± 5	16 ± 2
P2d8	13 ± 3	19 ± 5	12 ± 2

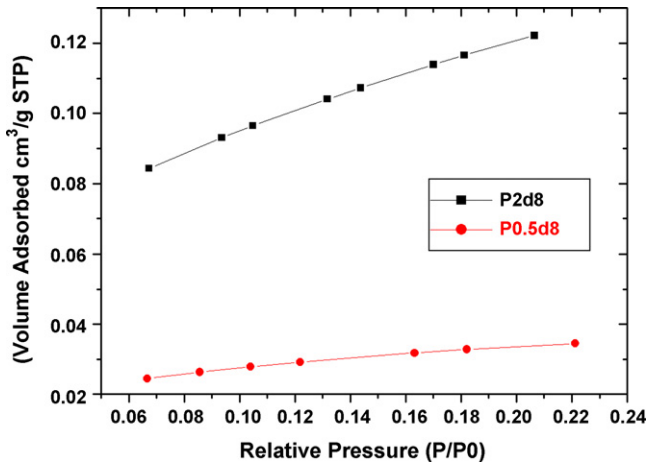

Fig. 5. Typical adsorption isotherm of krypton at 77 K on Pxdy films.

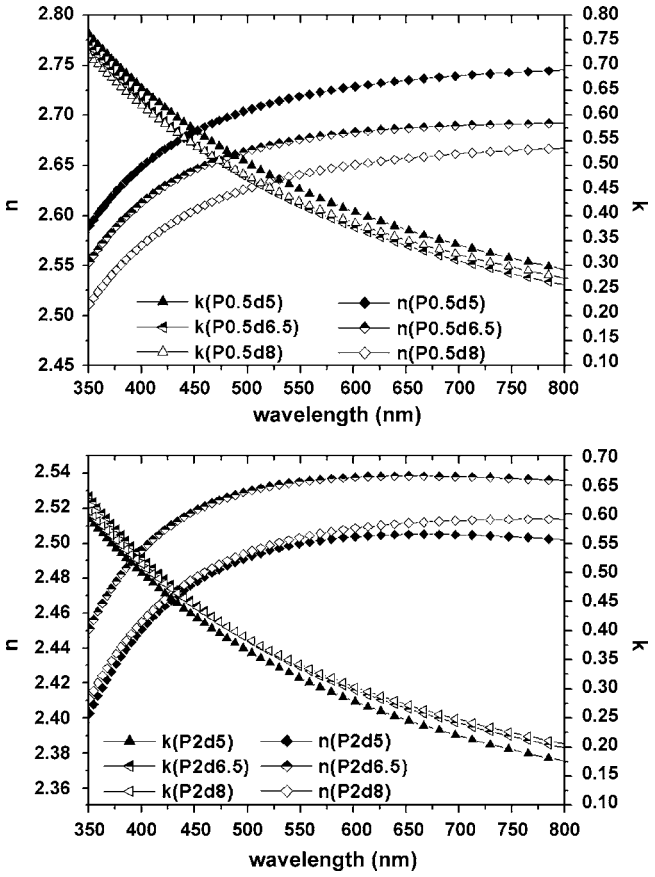

Fig. 6. Refractive (n) and absorptive (k) indices of Pxdy films in the whole visible spectral range.

Table 4
Comparison of the total film thickness obtained by the two optical models

Samples	Thickness (nm) model 1	Thickness (nm) model 2
P0.5d5	294	294
P0.5d6.5	295	295
P0.5d8	301	299
P2d5	323	318
P2d6.5	312	317
P2d8	305	303

The average porosity of (L_3) and (L_4) layers, due to the interstices between rods and domes (see Appendix B), can be expressed by:

$$p_3 = \frac{6\sqrt{3}L_3 + 3\sqrt{3}d - \pi(3L_3 + d)}{3\sqrt{3}(2L_3 + d)} \quad (2)$$

The average porosity for the whole film becomes:

$$p = \frac{6\sqrt{3}L_3 + 3\sqrt{3}d - \pi(3L_3 + d)}{3\sqrt{3}(2L_2 + 2L_3 + d)} \quad (3)$$

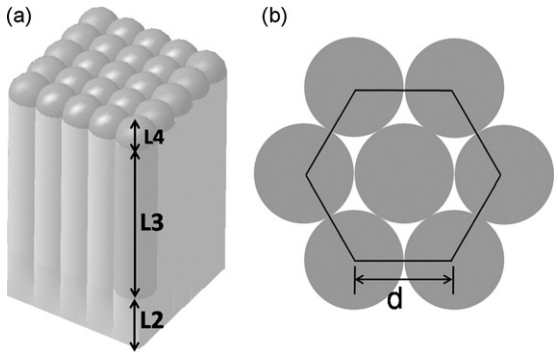

Fig. 7. Microstructural model of the films (a) 3-D view (b) detail of the hexagonal arrangement of the rods.

Finally, because the film surface is made up of the previous domes arranged in accordance to a hexagonal lattice, the roughness can be estimated (see Appendix C) by:

$R_a \approx 0.123d$

From expressions (1)–(3), we can see that the porosity, SEF and R_a can be calculated knowing only L_3 and d. L_3 can be directly determined from ellipsometry measurements, d can be obtained from X-ray measurements if we assume that the rods diameter is equal to the apparent crystallite size. This assumption seems checked because as it was said previously (see Section 4) the grain size is very close to crystallite size. Consequently the porosity, SEF and R_a were calculated and compared to the experimental values to check if the coherency of this model. The calculated and experimental values of the porosity, SEF and R_a are compiled in Table 5.

6. Discussion

Table 5 shows that the experimental values of the porosity, SEF and R_a are quite well estimated by the model. In this model the pore size is defined by the size of the interstices between cylindrical rods arranged in a compact layer. In this case the pore size for the porous films studied is about 15% of the rods diameter that means the pore size is generally less than about 2 or 3 nm. This porosity, which is difficult to reveal for 300 nm samples by TEM, SEM or AFM, is therefore a micro-porosity according to the IUPAC's definition.

The simplified representation of the film porosity given by the model fits with the transmission electron micrographs obtained for thinner films (50 nm thick) (Fig. 8). For 50 nm thick P0.5d5, the micrograph reveals a completely dense film. For P2d8 however, nanometric pores can be observed in between the crystallites, as predicted by the model. The 50 nm thick samples were directly deposited on a carbon layer covering a copper grid for microscopy, henceforth the set was transparent to electrons. The thickness and the substrate were then different from the previously studied 300 nm samples deposited on glass slides. It can be assumed however, the spinel oxide growths were not completely different from each other as shown in SEM images (Fig. 4), and it is reasonwise to say TEM images are representative of the 300 nm

Table 5
Comparison of experimental and calculated data related to the films microstructure

Samples	Average porosity (experimental) (%)	Average porosity (calculated) (%)	SEF (experimental) (m^2)	SEF (calculated) (m^2)	R_a (experimental) (nm)	R_a calculated (nm)
P0.5d5	1.0 ± 0.3	0.7 ± 0.6	2.0 ± 0.5	2 ± 1	2.1 ± 0.2	2.1 ± 0.2
P0.5d6.5	1.2 ± 0.2	1.1 ± 0.1	2.0 ± 1.0	2 ± 1.5	1.8 ± 0.2	1.8 ± 0.2
P0.5d8	2.5 ± 0.5	5.4 ± 0.6	30 ± 3	39 ± 10	1.9 ± 0.2	1.7 ± 0.2
P2d5	12.2 ± 0.3	9.2 ± 0.5	16 ± 2	46 ± 5	2.7 ± 0.2	2.6 ± 0.2
P2d6.5	12.5 ± 0.3	9.1 ± 0.3	53 ± 5	61 ± 11	1.9 ± 0.2	2.0 ± 0.2
P2d8	12.2 ± 0.2	9.2 ± 0.3	112 ± 11	84 ± 15	1.3 ± 0.2	1.5 ± 0.2

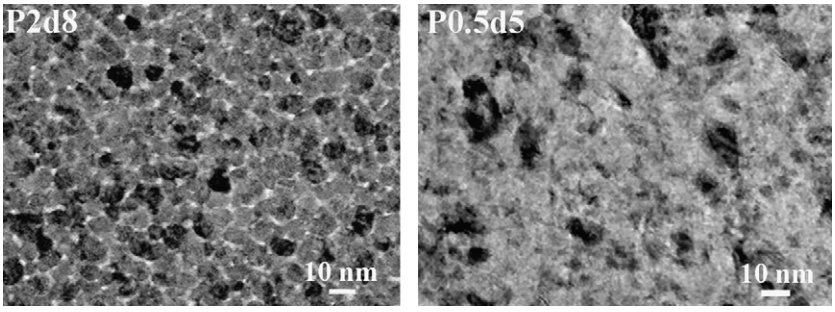

Fig. 8. Transmission electron micrograph of P2d8 and P0.5d5 50 nm films directly deposited on a carbon film.

films microstructure. Consequently it is not surprising that the surface enhancement factor measured by BET method is close to the values calculated from the model.

As it is generally assumed, the porosity results from shadowing effects for experimental conditions leading to a small mean free path λ, for the "atoms" in the argon plasma. Because λ is equal to $kT/\sqrt{2}\pi D^2 P$ (with k: Boltzman constant, T: absolute temperature, D: diameter of discharge molecules and P: argon pressure), such experimental conditions are encountered when argon pressure is high. In this case, "atoms" come to the substrate with an oblique incidence, the crystallites already formed, shade some small zones, which cannot grow as quick as the rest of the film. The angle of incidence also becomes higher by increasing the target–substrate distance. When the deposit temperature is not high, the lack of material in the previous depleted zones cannot be completely filled and leads to voids inside the film. Most of them become open micropores at the end of the film deposition. But some others can form close cavities. The model proposed, only takes into account open porosity but rules out the presence of such closed cavities. It is probably the reason why the agreement between the experimental and calculated values is not very satisfying for the porosity P2d*y* samples. These samples were in fact prepared in favourable conditions to develop close porosity.

Finally, the measured and calculated arithmetic roughness are also in a good corroborate, showing for such film the R_a value can be well estimated from the apparent crystallite size measurements.

7. Conclusion

$CoMnFeO_4$ thin films are stable materials, which enable the study of the influence of the RF sputtering experimental conditions on the microstructure of oxide films. Electronic or atomic force microscopy, together with gas adsorption techniques as well as ellipsometry, respectively, gave precise information about the fine microstructural characteristics of these films and their change in accordance with the operating sputtering parameters. It has been successfully demonstrated that films prepared with a sputtering argon pressure of 0.5 Pa and a target–substrate distance close to 5 cm are very dense films which display almost no pore. On the other hand, the samples obtained under higher pressure and/or longer distances are microporous with a mean pore size generally lower than 2 nm. The open part of porosity makes the specific surface area of the films quite high. Values up to about 75 m^2/g can be reached.

From these experimental data it was possible to propose a simple model to describe the main feature of the film microstructure. According to this model, the films are made of three layers. The first one, in contact with the substrate, has a relative density close to one hundred percent. The second layer, which covers the previous one, is made up of cylindrical rods set up in accordance with a hexagonal lattice. Its porosity is due to the interstices in the lattice. Hemispheric domes covering each rod make up the third layer, which displays a roughness directly related to the shape and the hexagonal arrangement of the domes.

The surface enhancement factor, the porosity and the arithmetic roughness, calculated from the model, are in corroboration with the experimental values of these parameters. The latter can be deduced from calculation knowing only the apparent crystallite size and the thickness of the porous layer, determined by X-ray diffraction and ellipsometry, respectively. The porosity is however slightly underestimated by the model for the samples prepared at high argon pressure. A close porosity, ruled out by the model, could then exist in such films.

Appendix A. Calculation of the surface enhancement factor of the film

A.1. Area calculation of the void spaces at the rod foot (S_V)

The unit cell of the hexagonal lattice (Fig. 7) is made up of 1 + (6/3) = 3 rods and its surface area is $(3\sqrt{3}d^2/2)$. The rod number by unit surface is therefore $(2/\sqrt{3}d^2)$.

The total surface area of the cylindrical rods per unit surface is $(2/\sqrt{3}d^2)\cdot(\pi d^2/4) = (\pi/2\sqrt{3})$. The total surface area of the void spaces between the rods is consequently $S_V = 1 - (\pi/2\sqrt{3})$ per unit surface.

A.2. Area calculation of the rod lateral surface (S_L)

The lateral surface area of one rod is $\pi d L_3$. The cumulated surface area S_L for the rods inside a unit surface is then:

$$S_L = \frac{2}{\sqrt{3}d^2}\cdot \pi d L_3 = \frac{2}{\sqrt{3}d}\cdot \pi L_3$$

A.3. Area calculation of the hemispheric domes (S_D)

Each dome of diameter d has a surface area of a half sphere having the same diameter. Per unit surface of film, the cumulative surface S_D of the domes is therefore:

$$S_D = \frac{2}{\sqrt{3}d^2}\cdot \frac{\pi d^2}{2} = \frac{\pi}{\sqrt{3}}$$

A.4. Surface enhancement factor (SEF)

The surface enhancement factor, SEF (i.e. the surface area on which gas adsorption can occur for a two dimensional unit surface of film) is the sum of S_V, S_L, S_D. This gives:

$$\mathrm{SEF} = \frac{(4L_3 + d)\pi + 2d\sqrt{3}}{2d\sqrt{3}}$$

Appendix B. Calculation of the average porosity of the film

B.1. Calculation of the total film volume per unit surface (V_T)

$$V_T = L_2 + L_3 + L_4 = L_2 + L_3 + \frac{d}{2} = \frac{2L_2 + 2L_3 + d}{2}$$

B.2. Calculation of the volume of oxide in the film (V_F)

The volumes of one cylindrical rod and the corresponding hemispherical dome per unit surface are $(2/\sqrt{3}d^2)\cdot(\pi d^2 L_3/4)$ and $(2/\sqrt{3}d^2)\cdot(\pi d^3/12)$ respectively. The oxide volume V_F in the whole film ($L_2 + L_3 + L_4$ layers) per unit surface is then:

$$V_F = L_2 + \frac{2}{\sqrt{3}d^2}\left[\frac{\pi d^2 L_3}{4} + \frac{\pi d^3}{12}\right] = \frac{6\sqrt{3}L_2 + \pi(3L_3 + d)}{6\sqrt{3}}.$$

B.3. Calculation of the porous volume (V_P)

$$V_P = V_T - V_F = \frac{6\sqrt{3}L_3 + 3\sqrt{3}d - \pi(3L_3 + d)}{6\sqrt{3}}$$

B.4. Calculation of the relative porosity (p)

$$p = \frac{6\sqrt{3}L_3 + 3\sqrt{3}d - \pi(3L_3 + d)}{3\sqrt{3}(2L_2 + 2L_3 + d)}$$

Appendix C. Calculation of the arithmetic roughness of the film

It is assumed that the AFM tip only probes the L_4 layer. The arithmetic roughness calculation takes therefore into account the topography of L_4 layer alone.

C.1. Calculation of the porous volume in L_4 layer

For a unit surface of L_4 layer, the total volume of the hemispheric domes is

$$V_D = \frac{2}{\sqrt{3}d^2}\cdot\frac{\pi d^3}{12} = \frac{\pi d}{6\sqrt{3}}.$$

These domes are included in a parallelepiped of $d/2$ high (Fig. A.1). Its volume is also $d/2$ because the surface area of its base is equal to one. The volume of the voids inside the parallelepiped is:

$$V_V = \frac{d}{2} - \frac{\pi d}{6\sqrt{3}}.$$

C.2. Calculation of the baseline position for arithmetic roughness calculation

The prism is virtually divided into two parts by a plane located at $(d/2 - z)$ from the base. In the upper part, the total volume of the truncated domes is

$$V_U = \frac{2}{\sqrt{3}d^2}\cdot\frac{\pi z^2}{3}\left[\frac{3d}{2} - z\right].$$

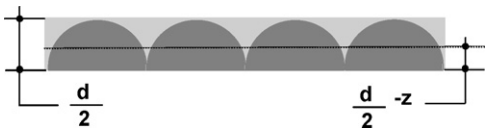

Fig. A.1. Cross-section of the L_4 layer showing the domes and the parallelepiped in which they are included.

In the lower part, the volume of the voids V_L is the difference between the total volume $(d/2 - z)$ and the volume of the lower parts of the domes $V_D - V_U = (\pi d/6\sqrt{3}) - (2/\sqrt{3}d^2)\cdot(\pi z^2/3)[3d/2 - z]$. Then:

$$V_L = \frac{d}{2} - z - \frac{\pi d}{6\sqrt{3}} + \frac{2}{\sqrt{3}d^2}\cdot\frac{\pi z^2}{3}\left[\frac{3d}{2} - z\right]$$

The value of z, defining the baseline for the R_a calculation, is such that $V_U = V_L$

$$\Leftrightarrow \frac{2}{\sqrt{3}d^2}\cdot\frac{\pi z^2}{3}\left[\frac{3d}{2} - z\right] = \frac{d}{2} - z - \frac{\pi d}{6\sqrt{3}} + \frac{2}{\sqrt{3}d^2}\cdot\frac{\pi z^2}{3}\left[\frac{3d}{2} - z\right]$$

$$\Rightarrow z = \frac{\left(3\sqrt{3} - \pi\right)d}{6\sqrt{3}}$$

C.3. Calculation of the arithmetic roughness (R_a)

R_a is equal to the sum of V_U and V_L when $V_U = V_L$. That means

$$R_a = 2\cdot\frac{2}{\sqrt{3}d^2}\cdot\frac{\pi z^2}{3}\left[\frac{3d}{2} - z\right] \quad \text{with } z = \frac{(3\sqrt{3} - \pi)d}{6\sqrt{3}}$$

$$\Rightarrow R_a \approx 0.123d$$

References

[1] S. Brunauer, P.H. Emmet, E. Teller, J. Am. Chem. Soc. 60 (1938) 209.
[2] P. Stefanov, G. Atanasova, T. Marinova, J. Gomez-Garcia, J.M. Sanz, A. Caballero, J.J. Morales, A.M. Cordon, A.R. Gonzalez-Elipe, Catal. Lett. 90 (2003) 195.
[3] S. Capdeville, P. Alphonse, C. Bonningue, L. Presmanes, Ph. Tailhades, J. Appl. Phys. 96 (2004) 6142.
[4] T. Yamazaki, T. Furuta, Y. Shen, C. Jin, T. Kikuta, N. Nakatani, Jpn. J. Appl. Phys. 45 (2006) 9180.
[5] I. Sandu, L. Presmanes, P. Alphonse, Ph. Tailhades, Thin Solid Films 495 (2006) 130.
[6] S.J. Martin, G.C. Frye, A.J. Ricco, T.E. Zipperian, IEEE Ultrasonic Symp. (1987) 563.
[7] V. Rouessac, R. Coustel, F. Bosc, J. Durand, A. Ayral, Thin Solid Films 495 (2006) 232.
[8] P. Revol, D. Perret, F. Bertin, F. Fusalba, V. Rouessac, A. Chabli, G. Passemard, A. Ayral, J. Porous Mater. 12 (2005) 113.
[9] A. Bourgeois, A. Brunet bruneau, V. Jousseaume, N. Rochat, S. Fisson, B. Demartes, J. Rivory, Thin Solid Films 366 (2004) 455.
[10] H. Xie1, J. Wei, X. Zhang, J. Phys. Conf. Ser. 28 (2006) 95.
[11] I. Chassaing, L. Presmanes, Ph. Tailhades, A. Rousset, Solid State Ionics 58 (1992) 261.
[12] G.E. Jellison, F.A. Modine, Appl. Phys. Lett. 69 (1996) 371.
[13] G.E. Jellison, F.A. Modine, Appl. Phys. Lett. 69 (1996) 2137.
[14] G.E. Jellison, V.I. Merkulov, A.A. Puretzky, D.B. Geohegan, G. Eres, D.H. Lowndes, J.B. Caughman, Thin Solid Films 68 (2000) 377.
[15] D.A.G. Bruggeman, Ann. Phys. (Leipzig) 24 (1935) 636.
[16] J.A. Thornton, J. Vac. Sci. Technol. 11 (1974) 666.